Direct NMR observation and DFT calculations of a hydrogen bond at the active site of a 44 kDa enzyme

Alexander Eletsky[a], Tim Heinz[a], Osvaldo Moreira[a], Alexander Kienhöfer[b], Donald Hilvert[b] & Konstantin Pervushin[a,*]

[a]*Laboratorium für Physikalische Chemie, Swiss Federal Institute of Technology, ETH Hönggerberg, CH-8093 Zürich, Switzerland;* [b]*Laboratorium für Organische Chemie, Swiss Federal Institute of Technology, ETH Hönggerberg, CH-8093 Zürich, Switzerland*

Abstract

A hydrogen bond between the amide backbone of Arg7 and the remote imidazole side chain of His106 has been directly observed by improved TROSY-NMR techniques in the 44 kDa trimeric enzyme chorismate mutase from *Bacillus subtilis*. The presence of this hydrogen bond in the free enzyme and its complexes with a transition state analog and the reaction product was demonstrated by measurement of ^{15}N-^{15}N and ^{1}H-^{15}N trans-hydrogen bond scalar couplings, $^{2h}J_{NN}$ and $^{1h}J_{HN}$, and by transfer of nuclear polarization across the hydrogen bond. The conformational dependences of these coupling constants were analyzed using sum-over-states density functional perturbation theory (SOS-DFPT). The observed hydrogen bond might stabilize the scaffold at the active site of BsCM. Because the Arg7-His106 hydrogen bond has not been observed in any of the high resolution crystal structures of BsCM, the measured coupling constants provide unique information about the enzyme and its complexes that should prove useful for structural refinement of atomic models.

Abbreviations: TROSY, transverse relaxation-optimized spectroscopy; DD, dipole-dipole coupling; CSA, chemical shift anisotropy; 2D, two-dimensional; TSA, oxabicyclic dicarboxylic acid transition state analog.

Introduction

The recent discovery of spin-spin scalar couplings across hydrogen bonds has made the direct detection of hydrogen bonds in biomacromolecules possible. This tool has been applied to nucleic acids (Dingley et al., 1998, 1999, 2000; Majumdar et al., 1999; Pervushin et al., 1998, 2000; Wohnert et al., 1999) and more recently to proteins (Cordier and Grzesiek, 1999; Cornilescu et al., 1999a,b; Hennig and Geierstanger, 1999; Liu et al., 2000a,b; Wang et al., 1999). In proteins, valuable structural information is often obtained from $^{3h}J_{NC'}$ couplings, from which secondary structure patterns can be deduced (Wang et al., 1999).

However, the magnitude of the coupling rapidly decreases with increasing H-bond length (Cornilescu et al., 1999b) and is typically smaller than 1 Hz (Dingley et al., 2000; Liu et al., 2000a,b). In contrast, large couplings between the hydrogen bond donating and accepting ^{15}N nuclei, $^{2h}J_{NN}$, in the range of 6–11 Hz and between ^{1}H nuclei and their ^{15}N acceptors, $^{1h}J_{HN}$, in the range of 2–4 Hz have been observed in DNA and RNA molecules (Dingley and Grzesiek, 1998; Pervushin et al., 1998) and for a hydrogen bond between two histidine side-chains in apomyoglobin (Hennig and Geierstanger, 1999). Nevertheless, direct detection of hydrogen bonds remains a challenging task in large proteins (m.w. > 30 kDa) due to the small magnitude of trans-hydrogen bond couplings and fast transverse relaxation of nuclear spins (Wang et al.,

1999). In the most cases only very limited structural interpretations of the observed values of the coupling constants are provided.

Here we report a general approach suitable for the experimental detection and analysis of N-H...N hydrogen bonds in large proteins using TROSY NMR together with quantum chemical DFT calculations. We apply this technique to the 44 kDa enzyme monofunctional chorismate mutase (EC 5.4.99.5) from *Bacillus subtilis* (BsCM) (Chook et al., 1994; Gray et al., 1990a,b, 1994; Rajagopalan et al., 1993). Chorismate mutase catalyses the Claisen rearrangement of chorismate to prephenate, the committed step in the biosynthesis of tyrosine and phenylalanine in bacteria, fungi, and higher plants (Chook et al., 1994; Rajagopalan et al., 1993). Despite more than two decades of studies on this novel biological rearrangement, the mechanism of the enzyme-catalyzed reaction remains unclear. Recently, X-ray crystal structures of BsCM bound to the *endo*-oxabicyclic transition state analogue were solved (Chook et al., 1994). Analysis of the active site structures has led to a general mechanistic hypothesis that the enzyme stabilizes the chairlike transition state geometry via a series of electrostatic and hydrogen-bonding interactions (Figure 1). Therefore it is of a critical importance to characterize the network of the hydrogen bonding interactions experimentally. Our NMR approach has revealed a structurally important hydrogen bond at the active site of this enzyme between Arg7 and His106. TROSY was exploited to measure the ^{15}N-^{15}N and ^{1}H-^{15}N trans-hydrogen bond scalar couplings, $^{h2}J_{NN}$ and $^{h1}J_{HN}$, and to transfer nuclear polarization across the hydrogen bond between the backbone amide of Arg7 and the imidazole side chain of His106. The sign of the both coupling constants was inferred from DFT calculations, which is otherwise very difficult to obtain experimentally for proteins of large molecular weight. Although this hydrogen bond was not identified in the crystal structures of the free enzyme or its complexes with various ligands, it can be formed by a 180° flip of His106 around its χ^2 angle. DFT calculations confirm the compatibility of the experimentally determined coupling constants with the amended structure. We propose that a combination of TROSY NMR with quantum chemical calculations represents a general approach for studying structural details and possibly mechanistic details in biomolecules by direct detecting of hydrogen bonds coupled with the analysis of conformational dependencies of the experimental values of the trans-H-bond couplings.
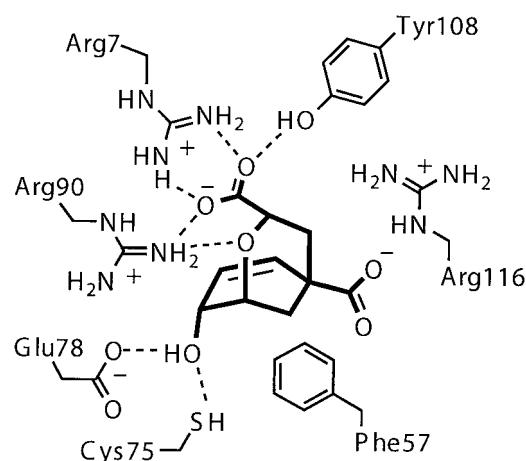

Figure 1. Schematic representation of the BsCM active site, showing the extensive array of hydrogen bonding and electrostatic interactions used to bind transition state analog 1 (bold). Arg7 forms a salt bridge with the secondary carboxylate group of the inhibitor. An analogous interaction with the enolpyruvate moiety of chorismate helps position the substrate within the active site for reaction.

Materials and methods

NMR sample preparation

^{15}N-labeled BsCM was produced in *E. coli* strain KA13 transformed with the pKET3-W plasmid (MacBeath and Kast, 1998; Mattei et al., 1999) using Bioexpress YBN (CIL) cell growth medium. The protein was purified as described in (Kast et al., 1996). To obtain complexes, 45 μl of 30 mM transition state analog (**1**) and, correspondingly, 1.3 mg of powdered prephenate were added to these protein solutions. In all samples pH = 6 was adjusted. Uniformly ^{15}N-, ^{13}C-, ^{2}H(<35%)-labeled BsCM (DL-BsCM sample) and uniformly ^{15}N-, ^{13}C-, ^{2}H-labeled BsCM (TL-BsCM sample) were produced according to similar protocols using Silantes d(<35%)C13N15 Medium and Celton medium, respectively.

NMR experiments were performed at 293 K on a Bruker AVANCE 600 MHz spectrometer. NMR data were processed with the program PROSA (Guntert et al., 1992). Chemical shifts are reported relative to DSS (sodium 2,2-dimethyl-2-silapentane-5-sulfonate).

J-coupling calculations by DFT

The hydrogen bonded conformation of the imidazole ring of His 106 to the backbone amide group of Arg7 was constructed by a 180° flip of His 106 around its

χ^2 angle in the X-ray structure of the BsCM (Ladner et al., 2000). The input structure for calculations was prepared by cutting a subset of atoms at C-C bonds from the X-ray structure corrected for the His106-Arg7 H-bond followed by addition of methyl groups resulting in charge neutral molecules. Thus, the input consisted of two molecules, (i) Ac-AlaNMe (Case et al., 2000) and (ii) 4-ethyl-imidazole in the ε-tautomeric form used to model the protein backbone around Arg7 and the side chain of His106, respectively (Figure 6). Calculations were carried out with the backbone angles $\Delta\chi^1 = (\chi^1 - 179.4°)$ and $\Delta\chi^2 = (\chi^2 - (-74.4°))$ of His106 set to fixed values with the steps in $\Delta\chi^1$ and $\Delta\chi^2$ of 5°, so that $\Delta\chi^1 = 0°$ and $\Delta\chi^2 = 0°$ correspond to the corrected structure. The remaining internal degrees of freedom were optimized with the Hartree–Fock method with a STO-3G basis set as implemented in the *Gaussian98* program (Frisch et al., 1998). The quantum chemical calculations of the scalar *J*-coupling constants were performed using sum-over-states density functional perturbation theory (SOS-DFPT) (Malkin et al., 1994) as implemented in the *deMon* program (St-Amant and Salahub, 1990). The function basis used for calculations is the *IGLO-III* (Kutzelnigg et al., 1991) except for the nitrogen atom, where we have used the *substitute* option with the parameter basis (*5,2;5,2*). The exchange correlation potential was *Perdew-86* (Perdew and Wang, 1992). In order to obtain a relatively good accuracy of the *J*-coupling constants the options for the numerical integration were set to *radial* 64 for the enlarged grid and *grid fine random* for the regular grids with the perturbation set on the $N^{\delta 2}$ atom of 4-ethyl-imidazole. Each calculation takes about 36 h on an 450 MHz SGI Octane2 and 18 h on 1.8 GHz Pentium 4 PC equipped with the fast Rambus memory.

Results

BsCM is a water soluble enzyme that catalyzes the rearrangement of chorismate to prephenate, a key step in the biosynthesis of the amino acids tyrosine and phenylalanine (Chook et al., 1994). It is a homotrimeric pseudo β-barrel surrounded by α-helices. The three solvent-accessible active sites are located at the subunit interfaces.

Direct experimental observation of the Arg7-His106 hydrogen bond

In the course of NMR spectroscopic studies of BsCM, we have assigned the chemical shifts of $^1H^N$, ^{15}N, $^{13}C^\alpha$ and $^{13}C^\beta$ resonances to individual residues in the free enzyme and its complexes with prephenate and with a transition state analog inhibitor (**1**) (Eletski, A., Kienhofer, A., Hilvert, D. and Pervushin, K., in preparation). A systematic attempt to reproduce structural shifts of ^1H, ^{15}N and ^{13}C resonances from their random coil values (e.g., de Dios and Oldfield, 1996; Le et al., 1995; Pardi et al., 1983) based on the high resolution crystal structures of the enzyme (Chook et al., 1994; Ladner et al., 2000) indicated the presence of an unusual hydrogen bond involving the active site residue Arg7. The backbone amide $^1H^N$ and ^{15}N resonances of Arg7 deviate from the corresponding random coil values by more than 3.5 and 10 ppm, respectively (Table 1). In the 3D structure of BsCM and its complexes, Arg7 is located in the middle of the B1 β-strand (residues 2–12) in a well-defined region of the structure. The guanidinium group of Arg7 is important for ligand binding, forming a salt bridge with the carboxylate group of the enolpyruvate side chain of chorismate (Chook et al., 1994; Lee et al., 1995) (Figure 1).

Based on the 3D structure, aromatic ring current effects are predicted to have a negligible effect on the chemical shifts of the backbone amide of Arg7. Given the known correlation between the $^1H^N$ shift and hydrogen bond strength (Cordier and Grzesiek, 1999; Wagner et al., 1983), unusual chemical shifts of Arg7 are most readily explained by hydrogen bonding. However, the most likely hydrogen bond acceptor, the imidazole group of His106, is not oriented appropriately in the 0.19 nm resolution crystal structures of BsCM complexed with prephenate or a transition state analog (Chook et al., 1994) or the 0.13 nm resolution structure of the free enzyme (Ladner et al., 2000). The unknown tautomeric state of His106 further precluded direct assignment of a hydrogen bond to Arg7 using standard geometrical criteria.

We therefore searched experimentally for a potential acceptor group for the Arg7 amide. The chemical shift of the ^{15}N spin to which Arg7 is hydrogen bonded was determined by a modified 2D $^{2h}J_{NN}$-correlation-[^{15}N-^1H]-TROSY experiment originally introduced to detect imino-to-imino hydrogen bonds in DNA base pairs (Pervushin et al., 1998). Because the spectral separation between the two ^{15}N spins across the hy-

Table 1. Experimental mean values rmsd[a] of the scalar coupling constants[b] for across the His106 $N^{\delta 1}$-Arg7 H^N hydrogen bond in BsCM and its complexes with a transition state analog (TSA) and prephenate, and the $^1H^N$ and ^{15}N chemical shifts of the donor Arg7 HN group

Quantity	Free BsCM	BsCM/TSA	BsCM/prephenate
$^{2h}J_{NN}$ (Hz)[b]	6.29 ± 0.04	6.1 ± 0.2	6.5 ± 0.2
$^{1h}J_{HN}$ (Hz)[b]	2.87 ± 0.15	n.d.	n.d.
Arg7 $^1H^N$ (ppm)	11.88	12.02	11.97
Arg7 ^{15}N (ppm)	130.6	130.1	131.3

[a]rmsd are obtained from seven independent measurements.
[b]$^{1h}J_{HN}$ coupling constants were determined only for unliganded ^2H, ^{15}N, ^{13}C-labeled BsCM.

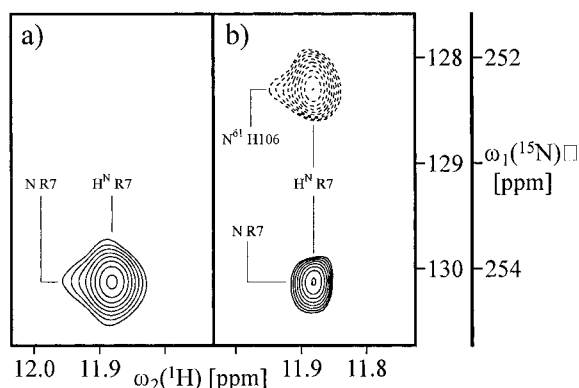*Figure 2.* (a) Expansion of the [^{15}N-^1H]-TROSY spectrum around the cross-peak of the Arg7 HN group. (b) The $^{2h}J_{NN}$-correlation-TROSY spectrum used to correlate the chemical shifts of the Arg7 HN group with the tertiary $N^{\delta 1}$ of His106 across the hydrogen bond. The spectrum was obtained according to the experimental scheme of Pervushin et al. (1998) with a magnetization transfer delay $\tau_2 = 25$ ms. In addition, the ^{15}N ϕ_1, ϕ_2 and 180° pulses in the middle of the $2^*\tau_2$ and $2^*\tau_3$ delays (see Figure 2 in Pervushin et al., 1998) were substituted by amplitude and phase modulated 800 μs gaussian-shaped pulses with two excitation/inversion maxima at 130 and 250 ppm. The ^{15}N carrier frequency was placed at 130 ppm. Due to double band splitting of the ^{15}N pulses, two ^{15}N frequency scales are indicated. The inner ^{15}N frequency scale applies to the diagonal resonances and the outer frequency scale corresponds to the ^{15}N frequency of the (negative) cross-peak (Dingley et al., 2000).
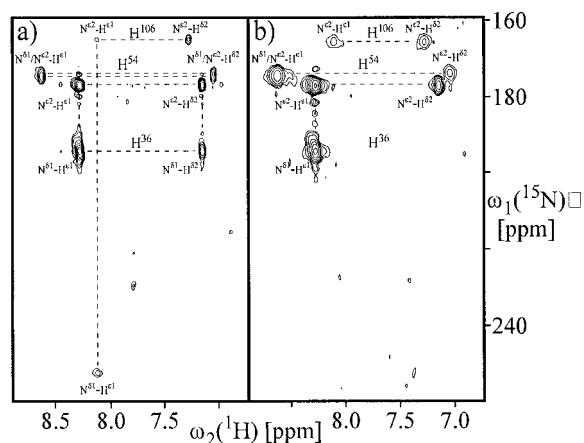

Figure 3. (a) The histidine region of the long-range [^{15}N-^1H]-HMQC spectrum (Pelton et al., 1993) of unliganded, ^2H,^{15}N,^{13}C-labeled BsCM. The spectrum was acquired over 2.5 days with 1024 scans, $t_{1max} = 8.4$ ms, $t_{2max} = 53$ ms, 512 and 112 complex points in the ^1H and ^{15}N dimensions, respectively. (b) The same region of the 2D TROSY-H(C)N spectrum (Riek et al., 2001) measured with unliganded, ^{15}N and ^{13}C-labeled BsCM. The spectrum was acquired over 2 days with 1024 scans, $t_{1max} = 9.9$ ms, $t_{2max} = 53$ ms, 512 and 72 complex points in the ^1H and ^{15}N dimensions, respectively.

drogen bond in BsCM is larger than in DNA, the magnetization transfer between the backbone ^{15}N spin of Arg7 and the $^{15}N^{\delta 1}$ spin of His106 was achieved with amplitude and phase modulated 800 μs gaussian-shaped pulses with two excitation/inversion maxima placed at 130 and 250 ppm; the ^{15}N carrier frequency was also maintained at 130 ppm. Figure 2b shows the 2D $^{2h}J_{NN}$-correlation-[^{15}N-^1H]-TROSY spectrum obtained with the unliganded enzyme. The chemical shift of the amide $^1H^N$ spin of Arg7 is correlated

with the chemical shifts of the directly attached ^{15}N spin (compare to Figure 2a) and a remote ^{15}N spin via the positive and negative cross-peaks, respectively. Although this experiment potentially allows simultaneous detection of $^{1h}J_{HN}$ coupling and determination of the sign of $^{1h}J_{HN}$ relative to the sign of $^1J_{HN}$, we were unable to detect magnetization stemming from the anti- TROSY component of the ^{15}N-^1H multiplet due to the extremely fast transverse relaxation. Nor did we observe direct splitting of the 2D correlation peak due to $^{2h}J_{NN}$ coupling. Instead, the positive sign of both $^{2h}J_{NN}$ and $^{1h}J_{HN}$ coupling constants was inferred from the quantum chemical calculations.
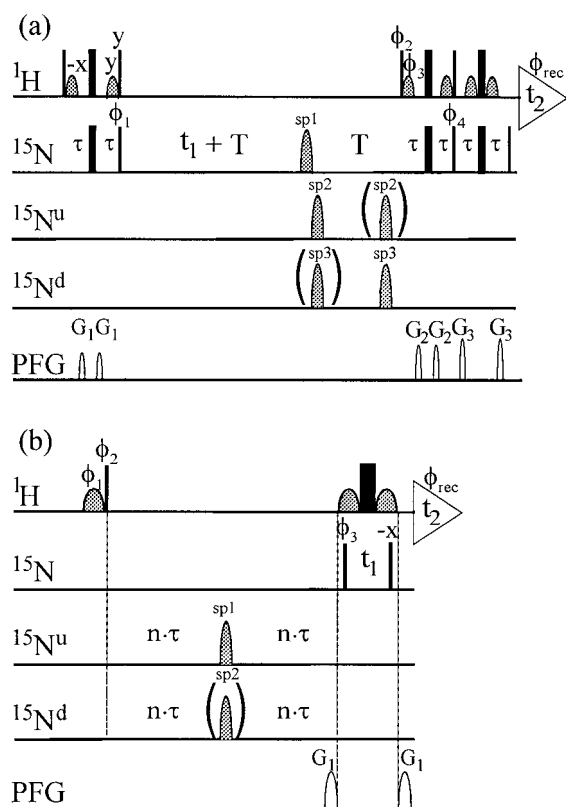
Figure 4. (a) and (b), schematic representation of the 2D $^{2h}J_{NN}$-quantitative-TROSY and $^{1h}J_{HN}$-quantitative- TROSY experiments to determine the $^{2h}J_{NN}$ and $^{1h}J_{HN}$ coupling constants, respectively. On the lines marked ^1H and ^{15}N, narrow and wide bars stand for non-selective 90° and 180° radio-frequency pulses applied at 4.78 ppm and 130 ppm, respectively. Water is flipped back at the end of the experiments by the 1.3 ms water-selective gaussian ^1H pulses. The line marked PFO indicates the pulsed magnetic field gradients applied along the z-axis: G_1, amplitude 30 G cm^{-1}, duration 1 ms; G_2, 40 G cm^{-1}, 1 ms; G_3, 48 G cm^{-1}, 1 ms. In (a), the delays are $\tau = 2.78$ ms and $T = 25$ ms. The following two-step phase cycling scheme was used: $\phi_1 = \{y, -x\}$; $\phi_2 = \{-y\}$; $\phi_3 = \{y\}$; $\phi_4 = \{-y\}$; $\phi_{rec} = \{y, -x\}$; x on all other pulses. To obtain a complex interferogram a second FID is recorded for each t_1 delay, with $\phi_1 = \{y, x\}$; $\phi_2 = \{y\}$; $\phi_3 = \{-y\}$; $\phi_4 = \{y\}$. During the delay T, the ^{15}N spins are inverted with phase modulated shaped pulses sp1, sp2 and sp3, where sp1 is the 1 ms gaussian on-resonance pulse; sp2 is the 2 ms I-BURP-2 pulse with the maximum excitation at 250 ppm; sp3 is the 2 ms I-BURP-2 with the maximum excitation at 10 ppm. Two data sets, I and II, were obtained in the interleaved manner. Data set I was measured without performing the bracketed pulses on the $^{15}N^d$ and $^{15}N^u$ lines, whereas data set II was obtained by running the experiment only with the bracketed sp2 and sp3 pulses. To calculate the $^{2h}J_{NN}$ coupling constant, a difference spectrum was constructed by subtracting data sets I and II. Data set II was then used as the reference spectrum. Equation 5 from Pervushin et al., 2000 was used to calculate $^{2h}J_{NN}$. In (b), the delay are $\tau = 2.78$ ms with n = 11. The phases are $\phi_1 = \{-x, x\}$; $\phi_2 = \{x, -x\}$; $\phi_3 = \{x\}$; $\phi_{rec} = \{x, -x\}$; x on all other pulses. The quadrature was obtained by setting $\phi_3 = \{y\}$ and repeating the experiment. sp1 and sp2 are the 0.5 ms gaussian 180° ^{15}N pulses with the maximum of excitation placed at 250 ppm and 10 ppm, respectively. Two data sets are obtained and processed as in (a).
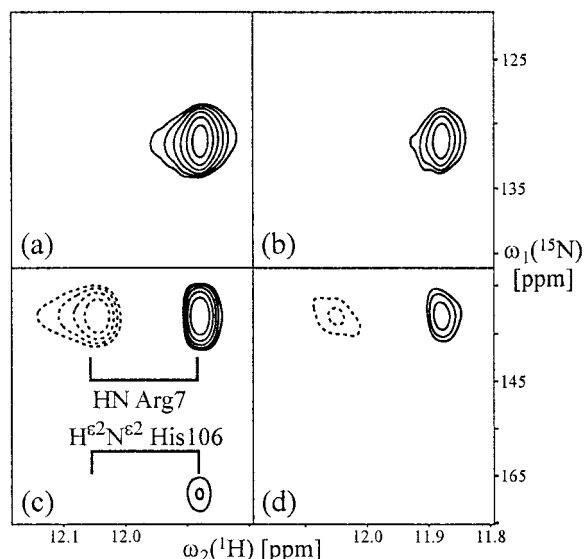

Figure 5. The reference (a) and difference (b) $^{2h}J_{NN}$-quantitative TROSY spectra and the reference (c) and difference (d) $^{1h}J_{HN}$-quantitative TROSY spectra measured with the experimental schemes of Figures 3a and 3b, respectively. The spectra were extracted from a single acquisition of the experiment. In (a) and (b) the experiment was recorded in 36 h with 128 scans and 1024 and 179 complex points in the ^1H and ^{15}N dimensions, respectively, and $t_{1max} = 5.3$ ms and $t_{2max} = 106$ ms. In (c) and (d) the experiment was recorded in 8 h with 64 scans and 1024 and 32 complex points in the ^1H and ^{15}N dimensions, respectively, and $t_{1max} = 3.2$ ms and $t_{2max} = 106$ ms. The spectra were recorded with the unliganded $^2H,^{15}N,^{13}C$-labeled BsCM. The [^{15}N-^1H] correlation cross-peaks for the HN Arg7 and $H^{\varepsilon2}N^{\varepsilon2}$ His106 groups are indicated.

Assignment of side chain resonances and tautomeric states of histidine

The ^{15}N resonance at 252 ppm was assigned to the imidazole $^{15}N^{\delta1}$ spin via a long range 2D [^{15}N-^1H]HMQC experiment (Pelton et al., 1993) and a variant of the 2D TROSY-H(C)N experiment (Riek et al., 2001). The sequence-specific assignment of the $^1H^{\varepsilon1}$ and $^1H^{\delta1}$ resonances of the three histidine residues in BsCM (residues 36, 54 and 106) was subsequently done using the NOESY spectrum. Despite the large size of the BsCM trimer (44 kDa), the imidazole ^{15}N and ^1H T_2's are large enough in the $^2H(<35\%)$-,^{15}N-,^{13}C-labeled protein that the $^2J_{N\delta1H\varepsilon1}$, $^2J_{N\varepsilon2H\varepsilon1}$, $^2J_{N\varepsilon2H\delta2}$ and $^3J_{N\delta1H\delta2}$ coupling constants produce observable correlations in the [^{15}N-^1H]-HMQC spectrum, thus allowing assignment of the $^{15}N^{\delta1}$, $^{15}N^{\varepsilon2}$, $^1H^{\delta2}$ and $^1H^{\varepsilon1}$ signals (Figure 3a). Since the 2D TROSY-H(C)N experiment also relies on the magnetization originating from the $^1H^{\delta2}$ and $^1H^{\varepsilon1}$ nuclei, uniform deuteration is no an option for

improving sensitivity of the spectra. Nevertheless, the large value of $^1J_{N\delta1C\epsilon1}$ as compared to $^2J_{N\delta1C\delta2}$ allows unequivocal assignment of the $^{15}N^{\delta1}$ and $^{15}N^{\epsilon2}$ chemical shifts, even when these have similar values, as usually observed for the charged tautomeric form. Together, the spectra of Figures 3a and 2b establish the tautomeric state of each individual histidine residue (Pelton et al., 1993) since the $^1H^{\delta2}$ spin is correlated only with the $^{15}N^{\epsilon2}$ spin in the TROSY-H(C)N spectrum, while in the [^{15}N-^1H]-HMQC spectrum the $^1H^{\delta2}$ spin exhibits cross-peaks with both the $^{15}N^{\epsilon2}$ and $^{15}N^{\delta1}$ spins. As expected from the fact that His106 is totally inaccessible to solvent, it adopts the unprotonated tautomeric form in which $N^{\epsilon2}$ bears a hydrogen. This assignment is further confirmed by the observation of an $^{15}N^{\epsilon2}$-$^1H^{\epsilon2}$ correlation cross peak in the 2D [^{15}N-^1H]-TROSY spectrum at 165 ppm. These experiments conclusively show that His106 is hydrogen bonded to the backbone amide of Arg7 via its $N^{\delta1}$ atom. In contrast, His36 and His54 are located on the surface of the protein and adopt charged tautomeric states, with both imino protons in fast exchange with water.

Quantitative measurements of $^{2h}J_{NN}$ and $^{1h}J_{HN}$ coupling constants

Novel 2D $^{2h}J_{NN}$-quantitative-[^{15}N,^1H]-TROSY and 2D $^{1h}J_{HN}$-quantitative-[^{15}N,^1H]-TROSY experiments (Figures 4a and 4b) were used to determine the value of the $^{2h}J_{NN}$ and $^{1h}J_{HN}$ coupling constant in free BsCM and BsCM complexed with prephenate and the transition state analog. The 2D $^{1h}J_{HN}$-quantitative-[^{15}N,^1H]-TROSY experiment of Figure 4b employs the slowly relaxing component of the imino ^1H doublet to relay magnetization via $^{1h}J_{HN}$ across the hydrogen bond to the tertiary ^{15}N of His106. Representative spectra used to measure $^{2h}J_{NN}$ and $^{1h}J_{HN}$ are shown in Figure 5. The derived coupling constants are reported in Table 1. Although the value of the $^{2h}J_{NN}$ coupling constant can be also estimated from the ratio of the cross-peak volumes in the spectrum of Figure 2b, the J-quantitative experiments provide better sensitivity (Pervushin et al., 2000). The gain in sensitivity comes from the fact that J-quantitative experiments employ only a unidirectional magnetization transfer between coupled spins, which requires twice as short a time delay compared to the chemical shift detection techniques. They also avoid sensitivity losses associated with the TPPI-type chemical shift detection and transverse relaxation during the incremental chemi-
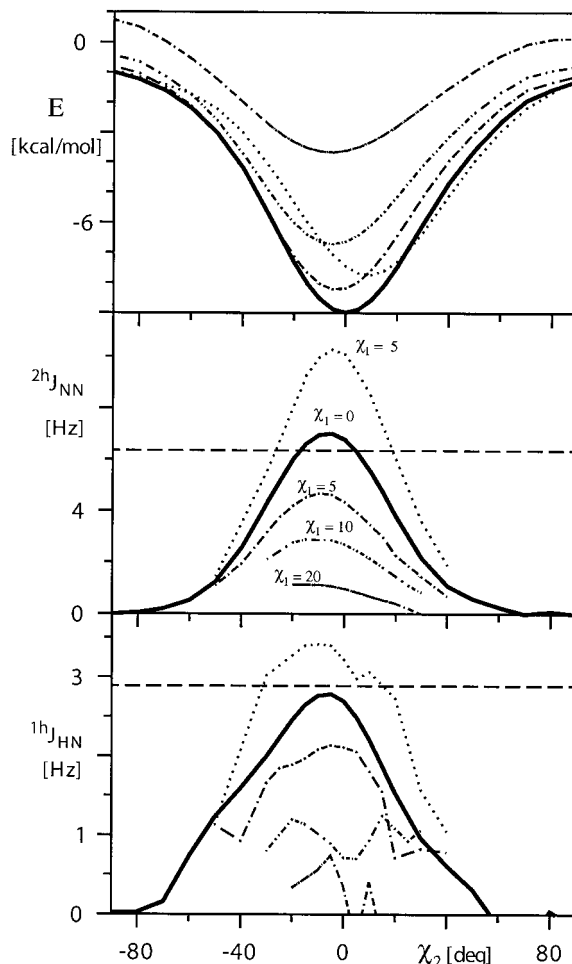

Figure 7. Computed relative conformational energy ΔE and scalar $^{2h}J_{NN}$ and $^{1h}J_{HN}$ coupling constants of Ac-Ala-NMe and 4-ethyl-imidazole molecules as a function of $\Delta\chi^1 = (\chi^1 - 179.4°)$ and $\Delta\chi^2 = (\chi^2 - (-74.4°))$ of His106, so that $\Delta\chi^1 = 0°$ and $\Delta\chi^2 = 0°$ correspond to the corrected X-ray structure (see Methods section). The dotted, solid, dot dashed, double-dot dashed and dot double-dashed lines correspond to $\Delta\chi^1 = -5°, 0°, 5°, 10°$ and $20°$, respectively. The experimental values of $^{2h}J_{NN}$ and $^{1h}J_{HN}$ coupling constants are marked by horizontal dashed lines.

cal shift evolution period. In agreement with the fact that the conformation of Arg7 is not significantly perturbed by the presence of ligand (Chook et al., 1994), the Arg7-His106 hydrogen bond is also observed in BsCM complexes with prephenate and TSA and it is characterized by similar coupling constants (Table 1).
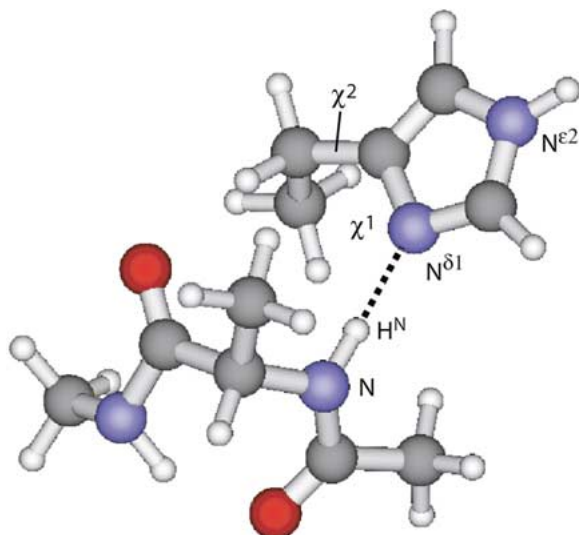
Figure 6. 3D geometries of the model system for which scalar coupling constants were calculated using density functional theory (DFT) methods as a function of the χ^1 and χ^2 torsion angles of His106. The Ac-Ala-NMe and 4-ethyl-imidazole molecules were constructed to model the backbone conformation of Arg7 and the side chain conformation of His106, respectively.
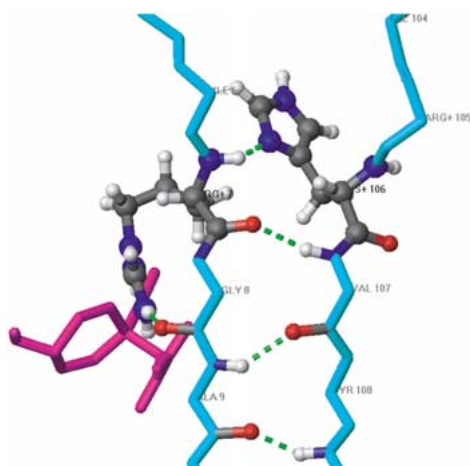

Figure 8. A model of the BsCM complex with prephenate (Chook et al., 1994) (PDB code lCOM, chain A) showing the structural context of the Arg7-His106 hydrogen bond. The parallel β-stands comprising residues Arg4 to Thr10 and Gln103 to Leu109 are displayed. Thick lines represent the backbone of all residues except Arg7 and His 106, for which all atoms are shown. Hydrogen bonds are indicated by dashed rods connecting the donor and acceptor atoms. All chemical bonds of the prephenate molecule are shown. Compared to its orientation in the crystal structure (Chook et al., 1994), the imidazole group of His106 is flipped by a 180° rotation around the χ^2 angle.

Conformational dependence of trans-hydrogen bond couplings

The χ^1 and χ^2 torsion angles of His106 were chosen as conformational variables defining the position of the hydrogen bond accepting imidazole ring relative to the hydrogen-bond donating amide group of Arg7. Figure 6 shows the 3D geometry of the two molecules, Ac-Ala-NMe and 4-ethylimidazole (see Methods), used to mimic the conformational arrangement of the Arg7-His106 hydrogen bond in the protein. The protein scaffold imposes strict limitations on the conformational freedom of the imidazole ring of His106 allowing practically only ∼180° flips of the imidazole moiety around χ^2 angle, compatible with the crystallographic electron density. Nevertheless, the calculated values of both $^{2h}J_{NN}$ and $^{1h}J_{HN}$ coupling constants are rather sensitive to small variations of the χ^1 and χ^2 angles as becomes apparent from Figure 7. The values of the $^{2h}J_{NN}$ coupling constant show a very clear Gaussian bell functional dependence on $\Delta\chi^2$ as a variable and $\Delta\chi^1$ as a parameter. The maximum of all Gaussian bell functions is shifted to about $\Delta\chi^2 = -5°$. Similar behavior is observed for the $^{1h}J_{HN}$ coupling, although in that case the precision of the calculations is apparently lower. For the orientation of the imidazole group found in the corrected X-ray structure (see Methods), good agreement between experimental values ($^{2h}J_{NN} = 6.5 \pm 0.2$ Hz and $^{1h}J_{HN} = 2.87 \pm 0.15$ Hz) and calculated values ($^{2h}J_{NN} = 6.8$ Hz and $^{1h}J_{HN} = 2.5$ Hz) of both couplings is obtained. At the negative value of $\chi^1 = -5°$ a significant increase of both coupling constants is observed resulting from the conformational clash between the imidazole and amide moieties accompanied by the increase of the conformational energy (Figure 7). Based on DFT calculations we can conclude that the orientation of the imidazole ring found in the corrected structure of BsCM is compatible with the experimental values of $^{2h}J_{NN}$ and $^{1h}J_{HN}$ coupling constants and that no further refinement is needed.

Discussion

Arg7 is one of the polar residues that line the active site of BsCM (Figure 1). Its guanidinium group forms a salt bridge with the C11 carboxylate of chorismate, which helps to position the enolpyruvyl side chain of the substrate for productive reaction. Replacement of this residue with a lysine or an alanine results in a

10^3 and 10^6 fold reduction in k_{cat}/K_m, respectively (Cload et al., 1996). The hydrogen bond that we observe between the backbone amide of Arg7 and the imidazole side chain of His106 is likely to contribute to the precise positioning of this active site residue.

Arg7 is located in the middle of the Bl strand (residues Met2 to Thr11) of the five-stranded β-sheet that forms the core of the BsCM protein. His106 immediately precedes the short B5 strand (residues Val107 to Leu109) to which B1 is paired. As shown in Figure 8, the hydrogen bond contributed by the imidazole side chain of His106 extends the interaction between the B1 and B5 strands and presumably helps to stabilize the protein scaffold in this region. Indeed, residues in the vicinity of Arg7 exhibit the lowest temperature factors in the crystal structure of BsCM, implying a comparatively rigid and well-ordered structure. The strict conservation of His106 in all known and putative AroH-class chorismate mutases further supports the structural importance of the Arg7-His106 hydrogen bond.

The use of TROSY NMR spectroscopy has allowed direct observation of a structurally important hydrogen bond connecting the backbone amide group of the active site Arg7 to the imidazole group of the remote His106 in the 44 kDa protein in solution. New TROSY-type experiments for the quantitative measurements of the trans-H-bond $^{2h}J_{NN}$ and $^{1h}J_{HN}$ scalar couplings were developed. In addition we propose the optimized TROSY-H(C)N experiment to establish the resonance assignment and tautomeric states of histidine side-chains. Since the magnetization transfer proceeds through one-bond couplings, this experiment represents a useful complement to conventional long-range [^{15}N-^{1}H]-correlation experiments traditionally used for the assignment of the histidine side-chain resonances (Pelton et al., 1993).

The presence of this H-bond was not suggested by the crystallographic analysis due to the incorrect selection of the two crystallographic ally indistinguishable orientations of imidazole rings. The compatibility of the Arg7-His106 hydrogen bond with the crystal structures of BsCM is demonstrated by an excellent agreement of the experimental and calculated values of both trans-hydrogen bond coupling constants based on the corrected X-ray structure of BsCM.

The availability of both $^{1h}J_{HN}$ and $^{2h}J_{NN}$ coupling constants is useful for refining the atomic models of BsCM since they are very sensitive functions of the relative geometrical arrangements of the donor and acceptor groups. Similar conclusions were made for the other types of the hydrogen bonds observed in proteins and nucleic acids (Barfield et al., 2001; Benedict et al., 2000; Dingley et al., 1999, 2001). Clearly, the described experiments are not limited to BsCM-detecting hydrogen bonds by NMR coupled with *ab initio* analysis is emerging as a general approach for elucidating structure and studying reaction mechanism in biomacromolecules.

References

Barfield, M., Dingley, A.J., Feigon, J. and Grzesiek, S. (2001) *J. Am. Chem. Soc.*, **123**, 4014–4022.

Benedict, H., Shenderovich, I.G., Malkina, O.L., Malkin, V.G., Denisov, G.S., Golubev, N.S. and Limbach, H.H. (2000) *J. Am. Chem. Soc.*, **122**, 1979–1988.

Case, D.A., Scheurer, C. and Bruschweiler, R. (2000) *J. Am. Chem. Soc.*, **122**, 10390–10397.

Chook, Y.M., Gray, J.V., Ke, H.M. and Lipscomb, W.N. (1994) *J. Mol. Biol.*, **240**, 476–500.

Cload, S.T., Liu, D.R., Pastor, R.M. and Schultz, P.G. (1996) *J. Am. Chem. Soc.*, 118, 1787–1788.

Cordier, F. and Grzesiek, S. (1999) *J. Am. Chem. Soc.*, **121**, 1601–1602.

Cornilescu, G., Hu, J.S. and Bax, A. (1999a) *J. Am. Chem. Soc.*, **121**, 2949–2950.

Cornilescu, G., Ramirez, B.E., Frank, M.K., Clore, G.M., Gronenborn, A.M. and Bax, A. (1999b) *J. Am. Chem. Soc.*, **121**, 6275–6279.

de Dios, A.C. and Oldfield, E. (1996) *Solid State NMR*, **6**, 101–125.

Dingley, A.J. and Grzesiek, S. (1998) *J. Am. Chem. Soc.*, **120**, 8293–8297.

Dingley, A.J., Cordier, F. and Grzesiek, S. (2001) *Concepts Magn. Reson.*, **13**, 103–127.

Dingley, A.J., Masse, J.E., Feigon, J. and Grzesiek, S. (2000) *J. Biomol. NMR*, **16**, 279–289.

Dingley, A.J., Masse, J.E., Peterson, R.D., Barfield, M., Feigon, J. and Grzesiek, S. (1999) *J. Am. Chem. Soc.*, **121**, 6019–6027.

Frisch, M.J. et al. (1998) Gaussian98 (Revision A.1), Gaussian, Inc., Pittsburgh PA.

Gray, J.V. and Knowles, J.R. (1994) *Biochemistry*, **33**, 9953–9959.

Gray, J.V., Golinellipimpaneau, B. and Knowles, J.R. (1990a) *Biochemistry*, **29**, 376–383.

Gray, J.V., Eren, D. and Knowles, J.R. (1990b) *Biochemistry*, **29**, 8872–8878.

Guntert, P., Dotsch, V., Wider, G. and Wüthrich, K. (1992) *J. Biomol. NMR*, **2**, 619–629.

Hennig, M. and Geierstanger, B.H. (1999) *J. Am. Chem. Soc.*, **121**, 5123–5126.

Kast, P., Hartgerink, J.D., Asif-Ullah, M. and Hilvert, D. (1996) *J. Am. Chem. Soc.*, **118**, 3069–3070.

Kutzelnigg, W., Fleischer, U. and Schindler, M. (1991) In *NMR: Basic Principles and Progress*, Vol. 23, Diehl, P., Fluck, E. and Kosfeld, E. (Eds.), Springer-Verlag, Berlin, pp. 165–262.

Ladner, J.E., Reddy, P., Davis, A., Tordova, M., Howard, A.J. and Gilliland, G.L. (2000) *Acta Crystallogr. Sect. D-Biol. Crystallogr.*, **56**, 673–683.

Le, H.B., Pearson, J.G., de Dios, A.C. and Oldfield, E. (1995) *J. Am. Chem. Soc.*, **117**, 3800–3807.

Lee, A.Y., Stewart, J.D., Clardy, J. and Ganem, B. (1995) *Chem. Biol.*, **2**, 195–203.

Liu, A.Z., Hu, W.D., Majumdar, A., Rosen, M.K. and Patel, D.J. (2000a) *J. Biomol. NMR*, **17**, 79–82.

Liu, A.Z., Hu, W.D., Majumdar, A., Rosen, M.K. and Patel, D.J. (2000b) *J. Biomol. NMR*, **17**, 305–310.

MacBeath, G. and Kast, P. (1998) *Biotechniques*, **24**, 789–794.

Majumdar, A., Kettani, A. and Skripkin, E. (1999) *J. Biomol. NMR*, **14**, 67–70.

Malkin, V.G., Malkina, O.L., Casida, M.E. and Salahub, D.R. (1994) *J. Am. Chem. Soc.*, **116**, 5898–5908.

Mattei, P., Kast, P. and Hilvert, D. (1999) *Eur. J. Biochem.*, **261**, 25–32.

Pardi, A., Wagner, G. and Wüthrich, K. (1983) *Eur. J. Biochem.*, **137**, 445–454.

Pelton, J.G., Torchia, D.A., Meadow, N.D. and Roseman, S. (1993) *Protein Sci.*, **2**, 543–558.

Perdew, J.P. and Wang, Y. (1992) *Phys. Rev.*, **B45**, 13244–13249.

Pervushin, K., Fernandez, C., Riek, R., Ono, A., Kainosho, M. and Wuthrich, K. (2000) *J. Biomol. NMR*, **16**, 39–46.

Pervushin, K., Ono, A., Fernandez, C., Szyperski, T., Kainosho, M. and Wüthrich, K. (1998) *Proc. Natl. Acad. Sci. USA*, **95**, 14147–14151.

Rajagopalan, J.S., Taylor, K.M. and Jaffe, E.K. (1993) *Biochemistry*, **32**, 3965–3972.

Riek, R., Pervushin, K., Fernandez, C., Kainosho, M. and Wuthrich, K. (2001) *J. Am. Chem. Soc.*, **123**, 658–664.

St-Amant, A. and Salahub, D.R. (1990) *Chem. Phys. Lett.*, **169**, 387–392.

Wagner, G., Pardi, A. and Wuthrich, K. (1983) *J. Am. Chem. Soc.*, **105**, 5948–5949.

Wang, Y.X., Jacob, J., Cordier, F., Wingfield, P., Stahl, S.J., Lee-Huang, S., Torchia, D., Grzesiek, S. and Bax, A. (1999) *J. Biomol. NMR*, **14**, 181–184.

Wohnert, J., Dingley, A.J., Stoldt, M., Gorlach, M., Grzesiek, S. and Brown, L.R. (1999) *Nucl. Acids Res.*, **27**, 3104–3110.